

Electronic Supplementary Information

Self-supported antimony tin oxide anode with Sb segregation promoted
atrazine removal

Xue Wang,^a Jia-Fang Xie,^{*a,b} Quan-Bao Zhao,^{*a,b} Qian Sun^{a,b}

^aCAS Key Laboratory of Urban Pollutant Conversion, Institute of Urban Environment,
Chinese Academy of Sciences, Xiamen, 361021, China. E-mail: jfxie@iue.ac.cn;
qbzhao@iue.ac.cn.

^bUniversity of Chinese Academy of Sciences, Beijing, 100049, China.

Experimental Methods

Materials

Antimony tin oxide ($\text{SnO}_2/\text{Sb}_2\text{O}_3$, 99.5%) was obtained from Aladdin Biochemical Technology Co.,Ltd (Shanghai, China) to make the SnO_2 -Sb anodes. Atrazine was purchased from Sigma-Aldrich. Acetonitrile, methanol, acetonitrile, formic acid (HPLC grade) were purchased from Oceanpak alexative chemical., Ltd. Furfuryl alcohol (FFA), p-benzoquinone (p-BQ), Chitosan, Amoxicillin (AMX), Tetracycline (TC), Bisphenol A (BPA), Norfloxacin (NOR) and Sulfadiazine (SZD) were purchased from Aladdin Biochemical Technology Co.,Ltd (Shanghai, China).

Tert-butyl alcohol (TBA), hydrochloric acid (HCl), paraffin oil, Sodium hydroxide (NaOH) and sodium sulfate (Na_2SO_4) were purchased from Sinopharm Chemical Reagent Co. Ltd (Shanghai, China). Carbon fiber (300-mesh) was obtained from Shenzhen Carbonene Technology Co., LTD. Polypropylene engineer fiber (10 mm) was obtained from Zhejiang Guangdeli non-woven fabric Co., LTD. All reagents were of analytical pure grade and used without further purification. Ultrapure water was used for the laboratory experiments.

Self-assembled ATO anode preparation

Preparation of EF-ATO anode:

Briefly, 0.01 g of polypropylene engineer fiber was added and stirred after 1.2 g of antimony tin oxide powder were combined. Different proportions of chitosan (1%, 5%, 10%, and 15%) were added to the powder and mixed. Then, the uniform mixture was slowly added to a circular mold (2.5 cm in diameter). Following the application of a hydraulic press with a uniaxial pressure of approximately 20 bar, the *EF-ATO* anode was sintered for six hours at 1000°C temperature in a muffle furnace. Subsequently, *EF-ATO* anode with pores were produced.

Preparation of CF-ATO anode:

Briefly, 0.18 g of carbon fiber was added and stirred after 1.2 g of antimony tin oxide powder were combined, and 0.2 mL of liquid paraffin was added to the powder and mixed. Then, the uniform mixture was slowly added to a circular mold (2.5 cm in diameter). Following the application of a hydraulic press with a uniaxial pressure of approximately 20 bar, the *CF-ATO* anode was sintered for six hours at 1000°C temperature in a muffle furnace. Subsequently, *CF-ATO* anode with pores were produced.

Anode characterization

A powder diffraction-meter (X'Pert Pro, PANalytical, Netherlands) measurements was equipped with Cu-K α radiation ($\lambda = 1.5444426 \text{ \AA}$). Data were collected in a 2-Theta range from 20° to 80° with a scan rate of 17° min⁻¹. The patterns were analyzed for crystalline phase and preferred orientation. Scanning electron microscopy (SEM, JEOL S-4800, Japan) was operated to investigate the material morphology. The texture analyzer (Universal TA, Shanghai Tengba) was applied to determine the hardness, fracturability, springiness, and cohesiveness of self-supported anodes. Brunauer-Emmett-Teller (BET) surfaces area and pore distribution of the samples were

determined by N₂ adsorption/desorption on a micromeritics analyzer (Quantachrome Autosorb iQ, USA) at -77 K in high-precision mode. X-ray photoelectron spectroscopy (XPS, Axis supra, Japan) was used to analyze the surface properties of the materials. Depth profiling was conducted using the Ar⁺ source operated at 5 kV and rastered over a 3 mm × 3 mm area. Each etching lasted for 300 s. Kelvin probe force microscopy (KPFM) measurement was conducted with a Bruker Dimension ICON in KPFM mode. The electron paramagnetic resonance (EPR) measurements were applied to determine the oxygen vacancy on a Bruker EMXplus-9.5/12 (Bruker, Germany). The solution pH was determined using a pH-meter (FE20, METTLER TOLEDO, USA) and recorded.

Electrochemical measurement

The single cell with three-electrode system was applied in this work. All experiments were performed in an electrocatalytic cell with 100 mL of electrolyte in a conventional three-electrode electrochemical cells driven by an electrochemical workstation (CHI 1140C, Chenhua, Shanghai, China). ATO anode served as the working electrode, a platinum sheet of 2 cm × 2 cm was used as the counter electrode, and Ag/AgCl sat. KCl electrode was used as the reference electrode. The working electrode and counter electrode were spaced at a consistent distance of 2 cm. The electrolyte utilized in this experiment was synthesized wastewater containing 20 mg L⁻¹ ATZ, which was continuously stirred at an agitation speed of 800 rpm. HCl (0.1 M) and NaOH (0.1 M) were used to adjust the pH of the electrolyte in pH-dependent experiments. When sampling from the degradation experiments, 1 mL of solution was taken from the electrolyte and filtered through a 0.45 μm PES filter before analyzed. All experiments were repeated at least twice, and the data shown were averaged.

The linear scanning voltammetry (LSV) experiments were measured in a 0.1 M Na₂SO₄ electrolyte solution. Scan rate of 0.01 V/s. Electrochemical impedance spectroscopy (EIS) measurements were carried out applying an ac signal of 5 mV amplitude with a frequency ranging from 10⁵ to 0.1 Hz at operating potential. All the electrochemical tests were performed at room temperature.

Ten consecutive degradation experiments were carried out using the same ATO anode to assess its recyclable stability. The experimental conditions were as follows: pH=6, 10 mA cm⁻², 0.1 M Na₂SO₄. In the cycling experiments, at the end of each cycling experiment, the electrodes were first drenched with ultrapure water and then oxidized in 0.1 M Na₂SO₄ at 0.1 A current for 10 min to remove possible residual contaminants on the surface.

Free radical quenching experiments were performed with tert-butanol (TBA), furfuryl alcohol (FFA), or p-benzoquinone (p-BQ). They were added to the electrolyte separately and the change in ATZ content was determined under optimal experimental conditions. Additionally, *in-situ* EPR (A300, Bruker, Germany) was used to confirm the presence of the aforementioned active species in the EO system. By using 5,5-dimethyl-1-pyrroline-N-oxide (DMPO) and 2,2,6,6-tetramethyl-4-piperidinyloxy (TEMP) to capture •OH, O₂⁻, and ¹O₂, respectively. The signal intensities of the three species were measured at 0 min, 10 min, and 20 min, respectively.

Detection and analysis method

The concentration of ATZ was determined by HPLC (Primaide, Hitachi, Japan) equipped with a DAD detector and a C18 column (4.6 mm × 250 mm, 5 μm). The mobile phases were acetonitrile/ 0.1 mM phosphoric acid solution (50: 50, v/v) with the flow rate of 1 mL·min⁻¹. Detection wavelength was set with λ = 223 nm. The samples after degraded were analyzed by a UPLC-MS/MS system with triple quadrupole mass spectrometer (ABI, 6500, USA), using electrospray ionization (ESI) in positive mode. Specifically, the mobile phase was consisted of ultrapure water (0.1%, formic acid, **A**) and acetonitrile (0.1%, formic acid, **B**) at a flow rate of 0.25 mL·min⁻¹. The ATZ concentration in samples was calculated according to Lamb-Bill's law. The removal rate of ATZ was further calculated by Eq. (1):

$$\text{Removal\%} = \frac{(C_0 - C_t)}{C_0} \times 100\% \quad (1)$$

where C₀ is the initial contaminant concentration (mg L⁻¹), C_t is the concentration of the contaminant at t in the degradation process (mg L⁻¹).

The reaction rate was evaluated by the pseudo-first-order kinetic model according to the following Eq. (2):

$$\ln \frac{C_0}{C_t} = k \times t \quad (2)$$

where C₀ is the initial contaminant concentration (mg L⁻¹), C_t is the concentration of the contaminant at t in the degradation process (mg L⁻¹), k is the apparent reaction rate constant (min⁻¹), and t is the time (min).

Energy consumption is one of the main parameters for assessing the feasibility of an effluent treatment system. The energy consumed by electrocatalytic oxidation for organic degradation treatment was estimated using electrical energy per order (E_{EO}) (kWh m⁻³). Generally, the E_{EO} values are calculated according to the following Eq. (3):

$$E_{EO} = \frac{E \times I \times t}{V \times l \times \left(\frac{C_0}{C_t}\right)} \quad (3)$$

where E is the cell potential (V), I is the current (A), V is the solution volume (L), t is the electrolysis time (h), C₀ is the initial pollutant concentration (mg L⁻¹), and C_t is the concentration measured at time t.

The relative contributions of •OH, •O₂⁻, and ¹O₂ to ATZ removal were evaluated with quenching experiments based on the equations (4)-(6), respectively:¹

$$R_{\bullet OH} = \frac{100 - RE_{TBA}}{(100 - RE_{TBA}) + (100 - RE_{FFA}) + (100 - RE_{pBQ})} \quad (4)$$

$$R_{\bullet O_2^-} = \frac{100 - RE_{pBQ}}{(100 - RE_{TBA}) + (100 - RE_{FFA}) + (100 - RE_{pBQ})} \quad (5)$$

$$R_{102} = \frac{100 - RE_{FFA}}{(100 - RE_{TBA}) + (100 - RE_{FFA}) + (100 - RE_{pBQ})}$$

(6)

Where R is the relative contribution ratio to ATZ removal; RE_{TBA} , RE_{pBQ} , and RE_{FFA} were the ATZ removal efficiency with specific quencher addition.

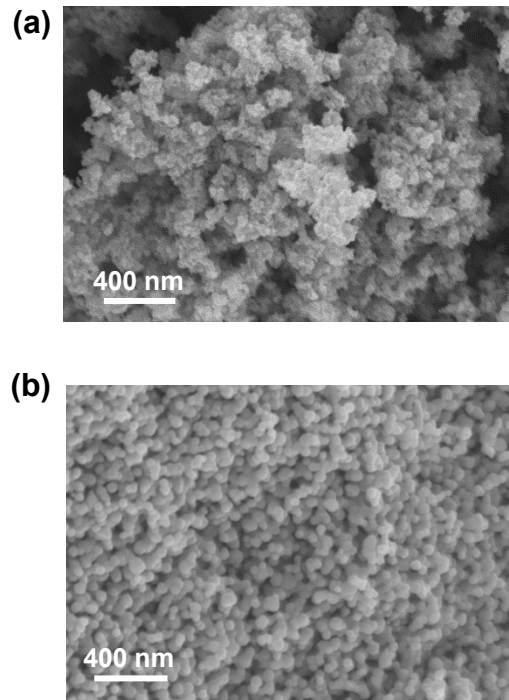


Figure S1. (a) SEM image of (a) initial ATO powder and (b) EF-ATO.

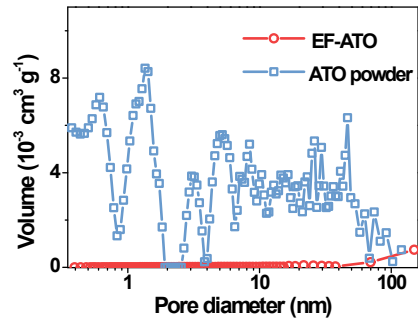


Figure S2. The corresponding pore distribution for initial ATO powder and EF-ATO.

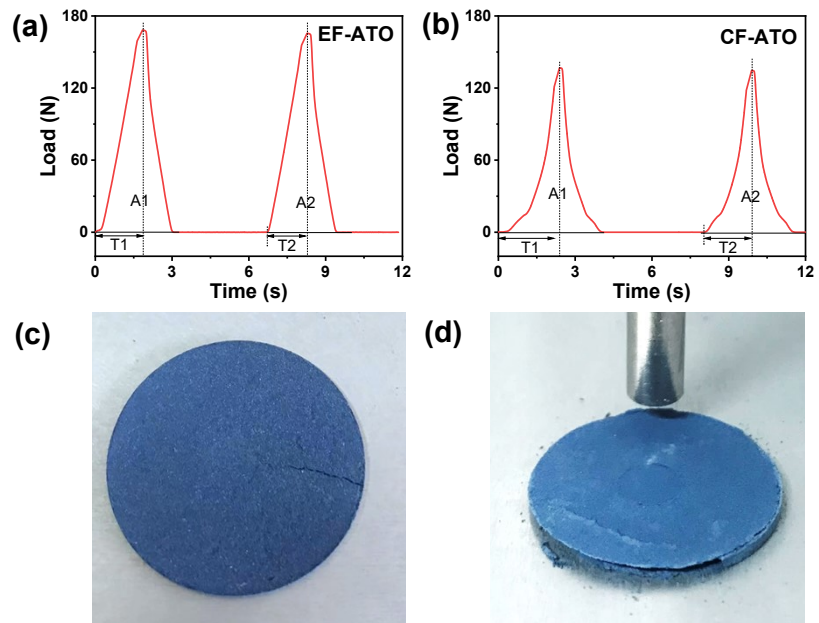


Figure S3. Texture analysis curves of (a) EF-ATO and (b) CF-ATO. Photos of (c) EF-ATO and (d) CF-ATO after texture measurement.

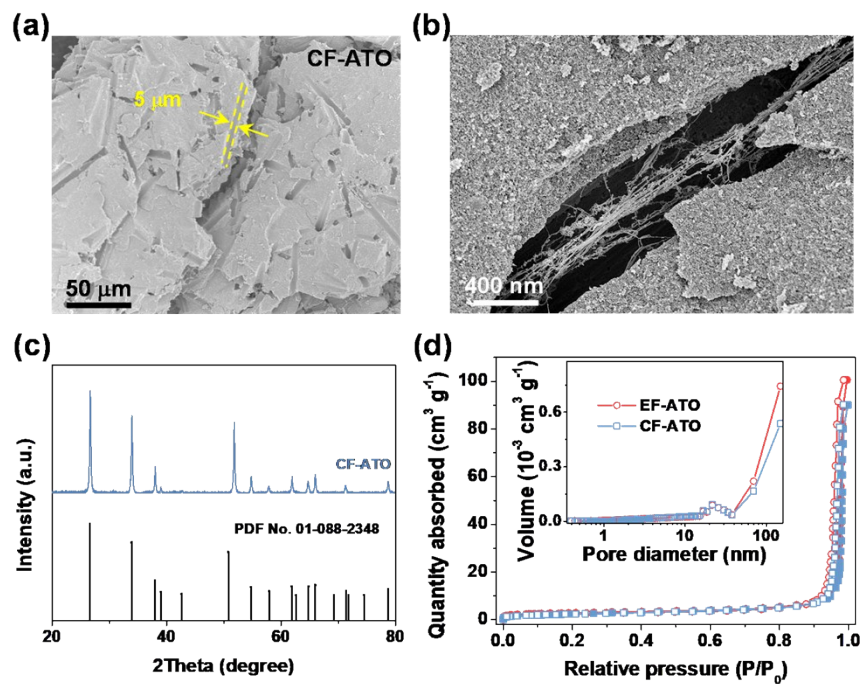


Figure S4. Structural properties of CF-ATO anode. (a, b) SEM images. (c) XRD pattern. (d) N₂ adsorption-desorption isotherms and corresponding pore distribution.

The same H3 hysteresis loop for EF-ATO and CF-ATO suggested both of their pores were mainly formed by particles stack.

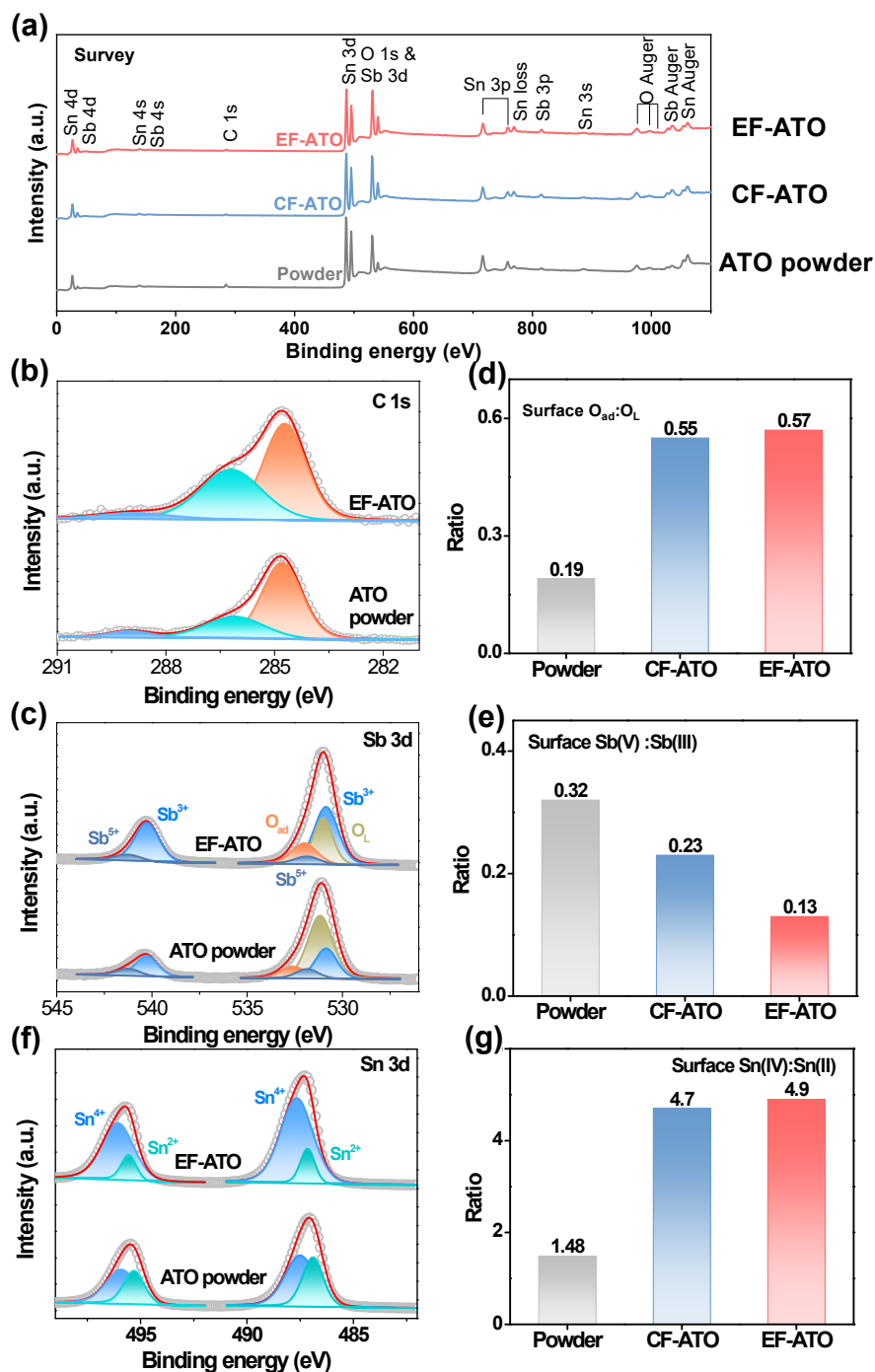


Figure S5. The XPS spectra for EF-ATO with CF-ATO and ATOPowder as comparison. (a) Survey spectra. High resolution spectra of (b) C 1s, (c) O 1s & Sb 3d, and corresponding (d) surface O_{ad}:O_L ratio and (e) Sb(V):Sb(III). (f) High resolution spectra of Sn 3d and (g) corresponding surface Sn(IV):Sn(II).

It is worthy mentioned that due to the overlap of O 1s and Sb 3d₅ peaks, Sb 3d₃ peaks needed fitted first. Then the location and area of peaks for Sb 3d₅ can be fixed according to the fitted Sb 3d₃. Finally, peaks belonging to O 1s could be added to fit the actual peak shape. CF-ATO shared similar change with EF-ATO compared to initial ATOPowder

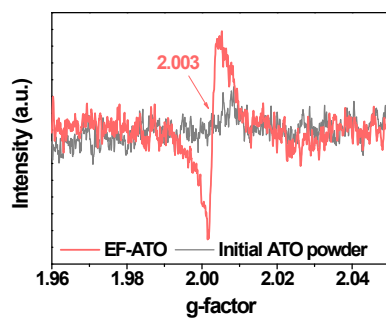


Figure S6. The calculated g-factor obtained by EPR for EF-ATO and initial ATO powder.

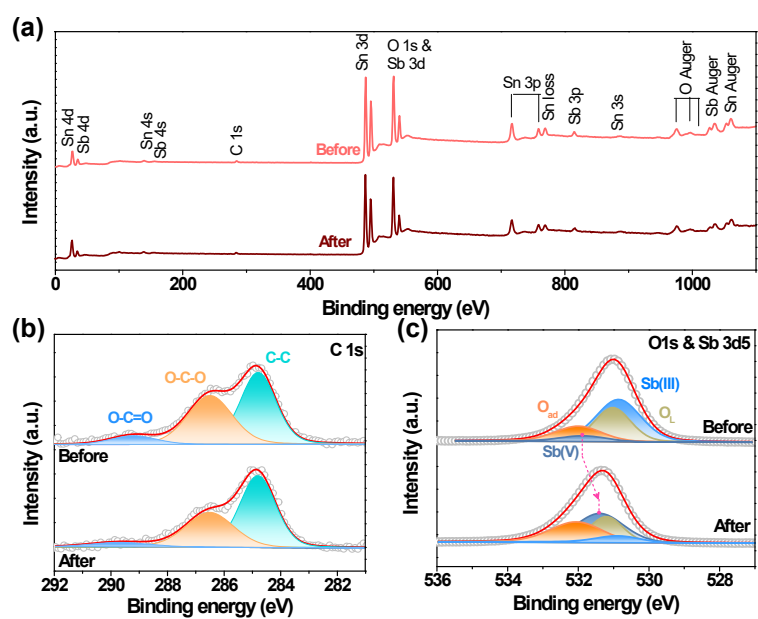


Figure S7. The XPS spectra for EF-ATO before and after EO process. (a) Survey spectra. (b) High-resolution C 1s spectra. (c) O1s& Sb 3d5.

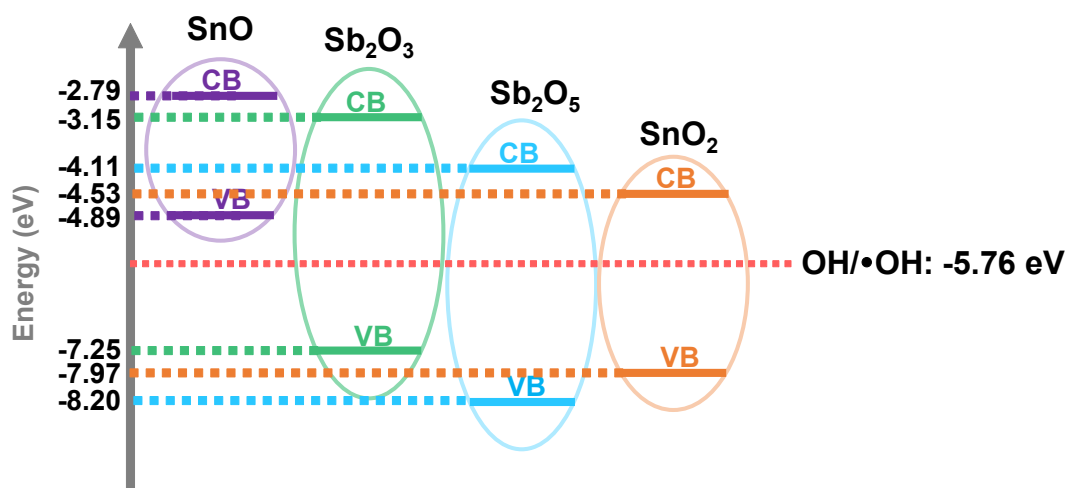


Figure S8. The band structure of metal oxides involved in EF-ATO. The data of band energy came from the references.²⁻⁵

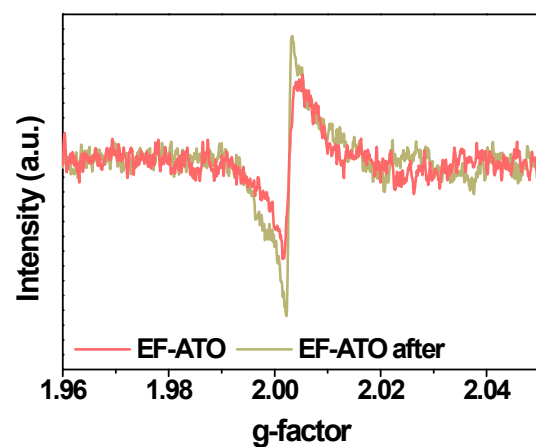


Figure S9. The calculated g-factor obtained by EPR for EF-ATO before and after EO process.

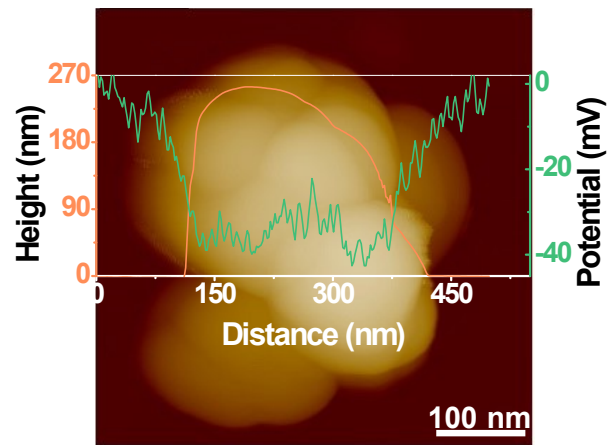


Figure S10. KPFM image with linear height and surface potential distribution for tin oxide powder.

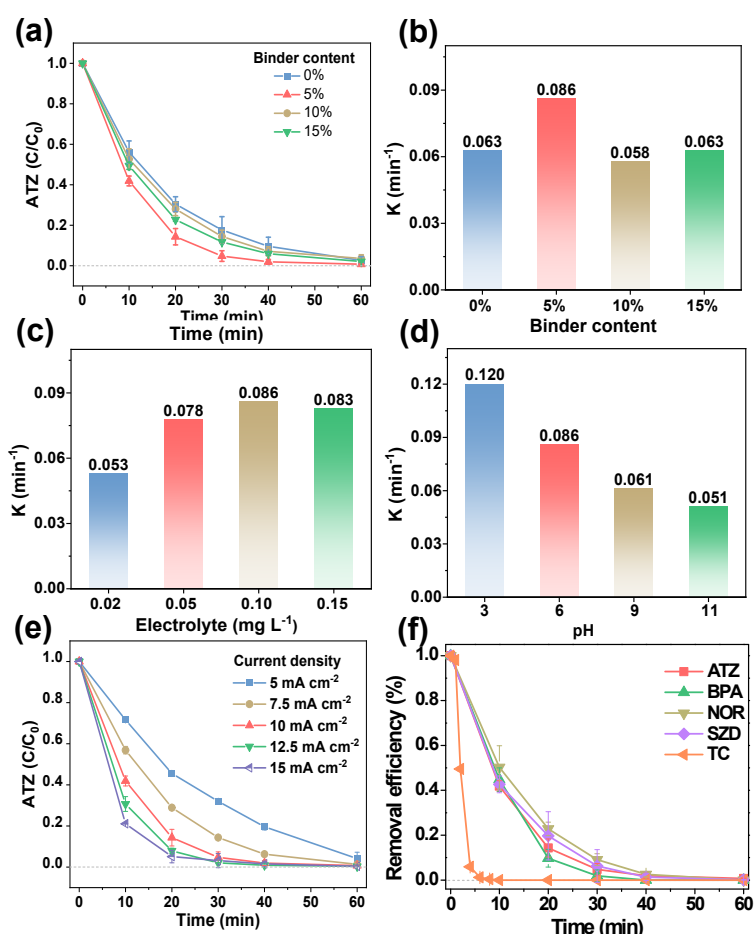


Figure S11. Influence factors on the EO process with EF-ATO. (a) Removal efficiency and (b) corresponding removal rate constant under a series of binder contents. Removal rate constant under a series of electrolyte (c) concentration and (d) pH. (e) Removal efficiency under a series of current densities. (f) Removal efficiency of several persistent organic pollutants. If not specified, experimental conditions: $C_0 = 20 \text{ mg L}^{-1}$, $j = 10 \text{ mA cm}^{-2}$, $\text{pH} = 6$, and Na_2SO_4 concentration = 0.1 M .

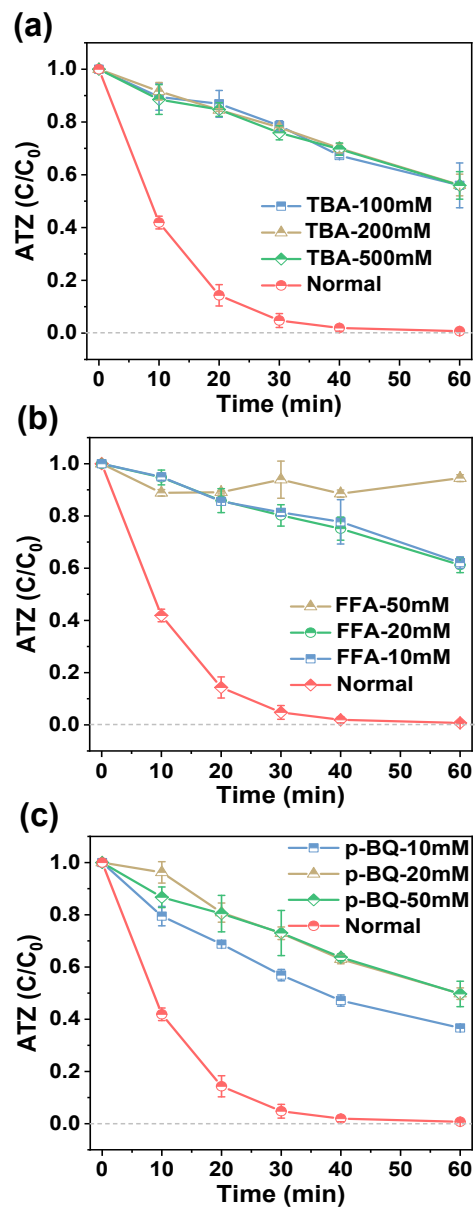


Figure S12. Quenching experiments using (a) TBA, (b) FFA, and (c) p-BQ with three concentrations.

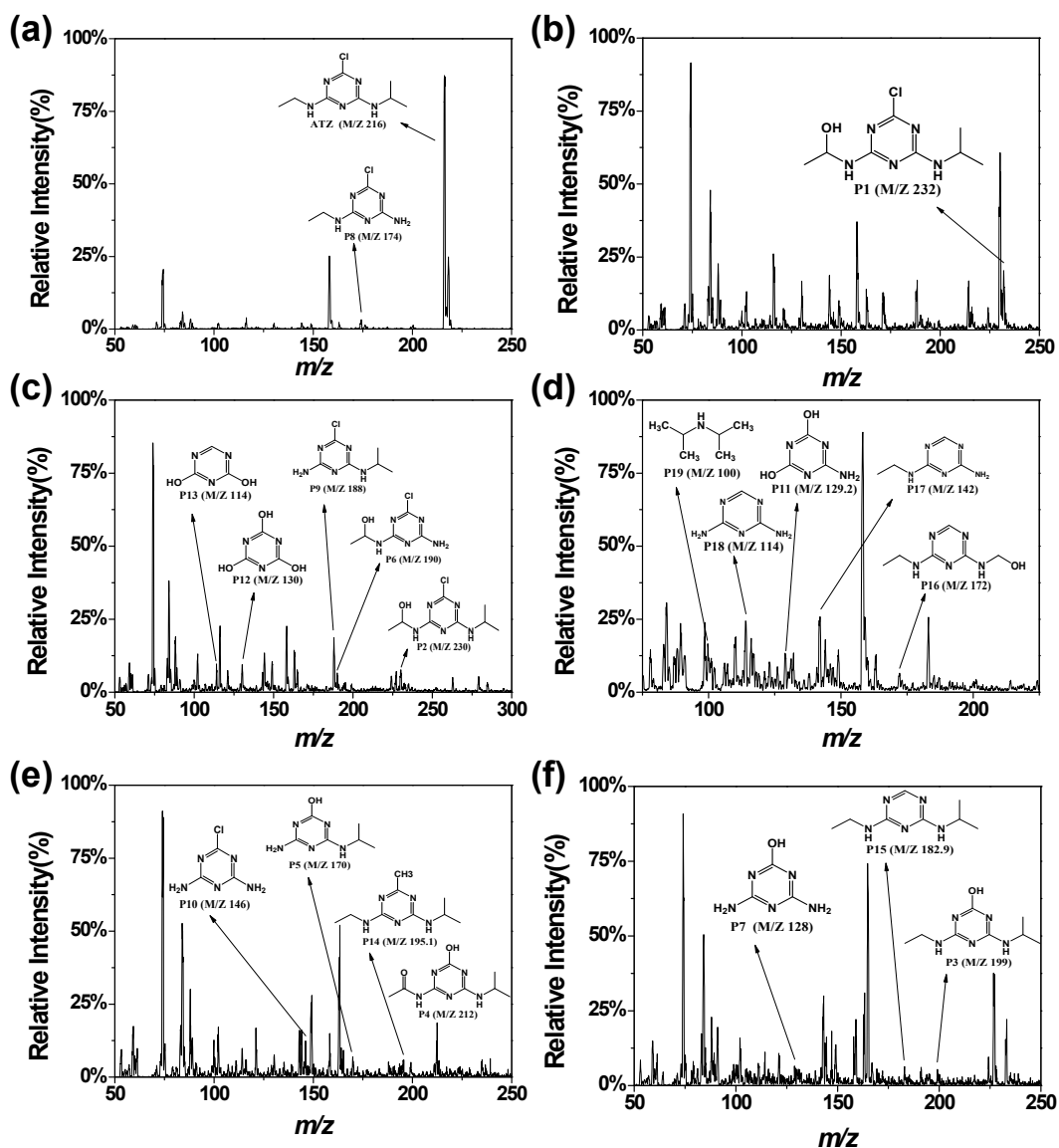


Figure S13. Spectra of ATZ degradation products by the UPLC-MS/MS system with triple quadrupole mass spectrometer.

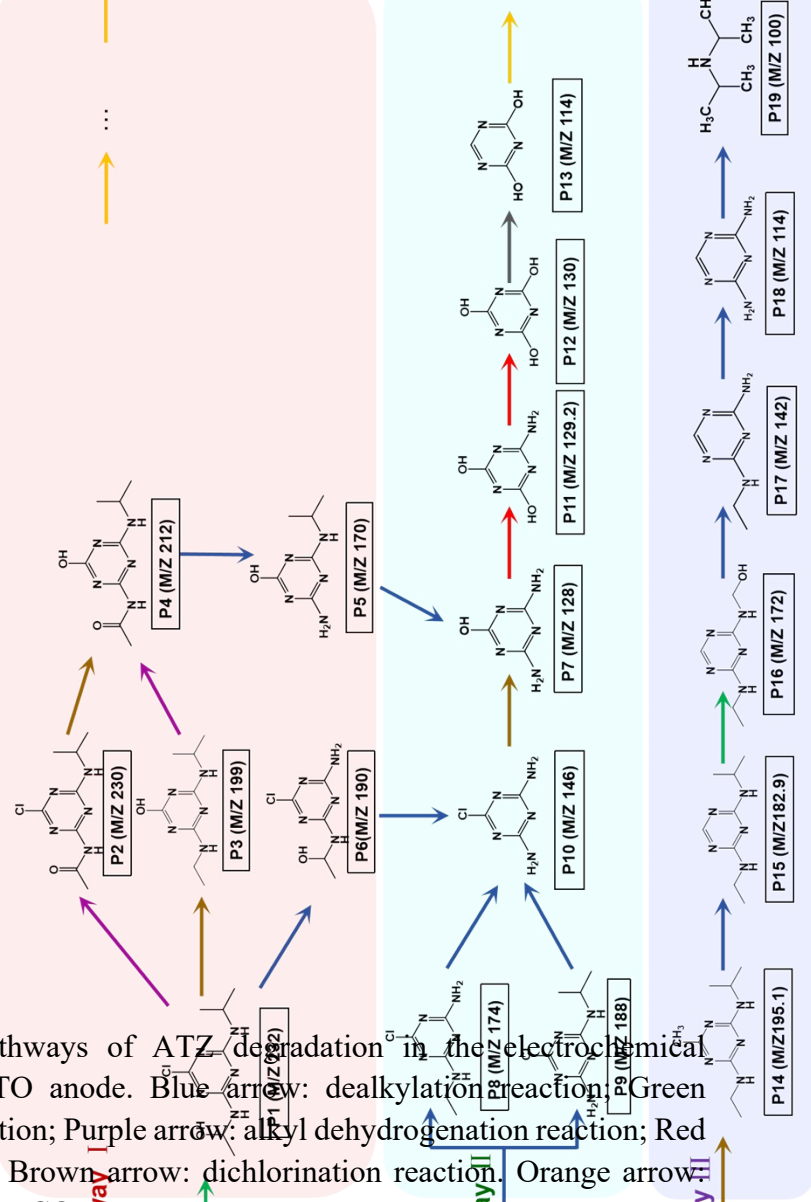


Figure S14. The possible pathways of ATZ degradation in the electrochemical oxidation process with EF-ATO anode. Blue arrow: dealkylation reaction; Green arrow: alkyl hydroxylation reaction; Purple arrow: alkyl dehydrogenation reaction; Red arrow: hydroxylation reaction; Brown arrow: dichlorination reaction. Orange arrow reactions leading to final product CO_2 .

The available data suggests that there are three main pathways for the degradation of atrazine in the electrochemical oxidation process with EF-ATO anode. Pathway I involve alkyl hydroxylation to produce P1 (m/z 232), P1 undergoes alkylation, dechlorination and hydroxylation to form P2 (m/z 230) and P3 (m/z 189), respectively. P2 and P3 are further side-chain dechlorination/alkylation and dealkylation to form intermediates P4 (m/z 212), P5 (m/z 170) and P7 (m/z 230). At the same time, a small part of P1 is dealkylated to form P6 (m/z 190) and further P10 (m/z 146). In route II, ATZ generates P8 (m/z 174) and P9 (m/z 188) by side chain dealkylation,⁶ and P8 and P9 are further formed by side chain dealkylation to form the intermediate product P10 (m/z 146). P10 undergoes a series of side chain dechlorination, hydroxylation, and re-dehydroxylation reactions to form the final product P13 (m/z 114). In pathway III, the ATZ is first dechlorinated to form P14 (m/z 195.1), then dealkylated to form P15 (m/z 182.9), further alkylated and dealkylated to form P16 (m/z 172), P17 (m/z 142) and P18 (m/z 114), and finally ring-opening to form P19 (m/z 100).⁷ Intermediates in each pathway have the potential to transform into each other and eventually oxidize and degrade to small molecule organics or completely mineralize to carbon dioxide and water.

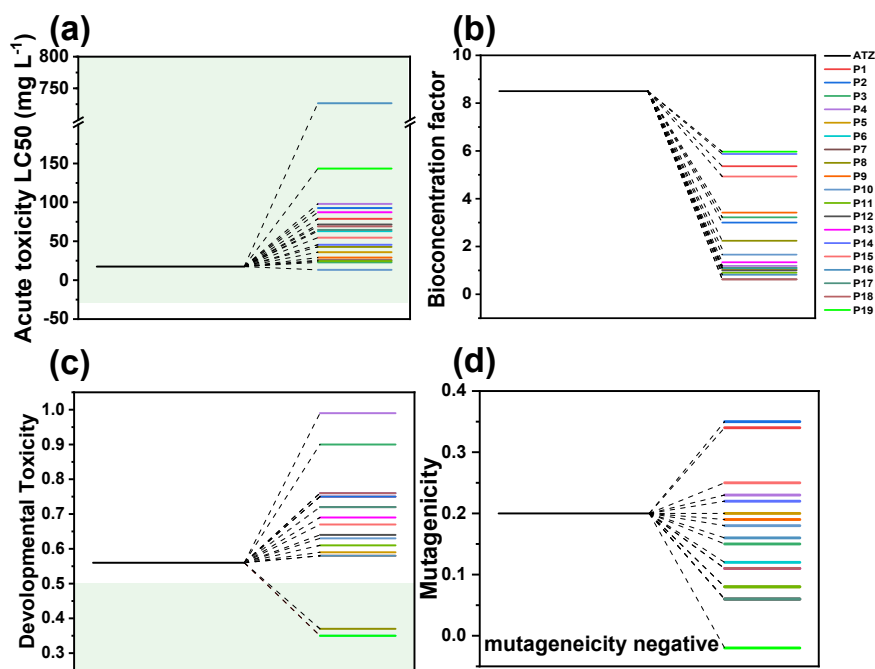


Figure S15. Toxicity evaluation of ATZ and its 19 degradation intermediate products. (a) Acute toxicity, (b) bioaccumulation factor, (c) developmental toxicity, and (d) mutagenicity.

The acute toxicity of ATZ and its degradation intermediates was assessed using the semi-lethal concentration of *Daphnia magna* LC50 within 48 hours. In addition, we investigated the bioaccumulation factors, developmental toxicity, and mutagenicity of ATZ and its metabolites. In the LD50 (LC50) of *Daphnia magna* (Fig. S11a), only one intermediate (P10) showed high toxicity after catalytic degradation, and the toxicity of all other intermediates was significantly lower than that of ATZ. This indicates that the acute toxicity is reduced during electrocatalytic degradation. In Fig. S11b, the bioaccumulation coefficient of all intermediates is much lower than that of ATZ. The decrease of bioaccumulation factor indicates that the accumulation ability of ATZ in the organism is reduced during the degradation process. In addition, the three intermediates P6, P8 and P19 are non-toxic to development, and the developmental toxicity of the remaining 16 intermediates is higher than that of the ATZ parent compound (Fig. S11c). Fig. S11d shows that although a small number of intermediates have higher mutagenic values than ATZ, all intermediates are considered negative. Thus, as the toxicity of ATZ gradually decreases the electrochemical oxidation process with EF-ATO anode is a feasible method for treating ATZ wastewater.

Table S1. The specific surface area of EF-ATO and initial ATO powder.

Anode	Specific surface area (cm² g⁻¹)	Average pore diameter (nm)	Pore volume (cm³ g⁻¹)
ATO powder	49.47	19.26	0.2561
EF-ATO	9.66	60.81	0.1468

Table S2. The mechanical strength of EF-ATO and CF-ATO.

Anode	Hardness	Fracturability	Springiness	Cohesiveness	Chewiness
	N	N			N
CF-ATO	140.35	ND	0.74	0.95	99.48
EF-ATO	172.82	162.97	0.82	0.95	134.74

ND: can not be detected.

Table S3. Recent anodes for ATZ removal.

No.	Material	Pollutant mass	Electrolysis condition	Removal efficiency	Time	Kinetics (min ⁻¹)	Ref.
1	Ti/SnO ₂ -Sb ₂ O ₅ /PbO ₂	15 mg L ⁻¹	40 mA cm ⁻²	100%	120 min	NM ^a	8
2	Ti/PbO ₂ -Co-Sm	20 mg L ⁻¹	20 mA cm ⁻²	92.6%	180 min	0.014 min ⁻¹	9
3	BDD	50 mg L ⁻¹	20 mA cm ⁻²	90%	60 min	0.002 min ⁻¹	10
4	MnCe-CM	4.3136 mg L ⁻¹	60 L m ⁻² h ⁻¹	99.9%	40 min	1.62 s ⁻¹	11
5	Ti/RuO ₂ -IrO ₂	25 mg L ⁻¹	20 mA cm ⁻²	89.23%	60 min	0.0383 min ⁻¹	12
6	Ti/IrO ₂ anode	3.5 mg L ⁻¹	15 mA cm ⁻²	95%	40 min	NM ^a	13
7	Bi-doped SnO ₂ -Ti _n O _{2n-1}	2.1568 mg L ⁻¹	3.5 V/SHE	100%	HRT 3.6 s	NM ^a	14

8	Sb, Ce co-doped SnO ₂ REM	5.392 mg L ⁻¹	545 A m ⁻²	100%	HRT 9 s	0.062 min ⁻¹	15
9	SnO ₂ -Bi-REM	2.1568 mg L ⁻¹	10 mA cm ⁻²	99%	100 mL min ⁻¹	NM ^a	16
10	EF-ATO	20 mg L ⁻¹	10 mA cm ⁻²	95%	30 min	0.086 min ⁻¹	This work

^a: not mentioned.

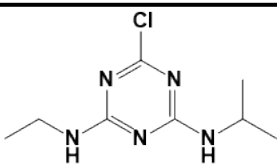
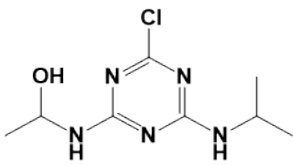
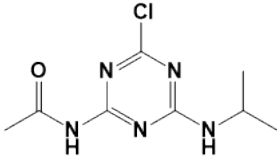
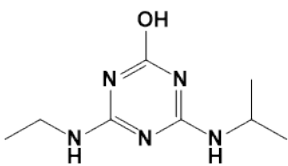
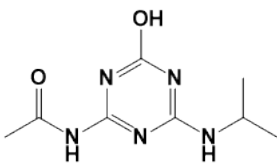
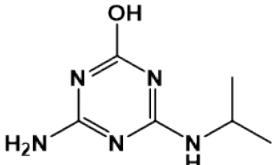
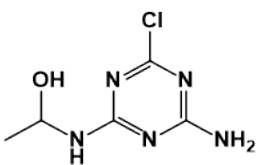
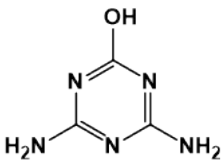
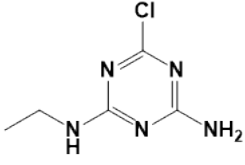
Table S4. Electrochemical impedance parameters obtained by EIS fitting.

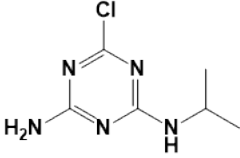
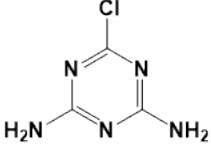
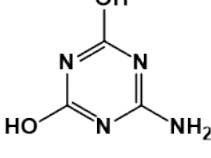
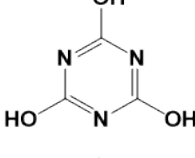
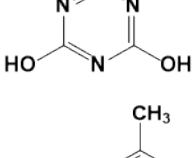
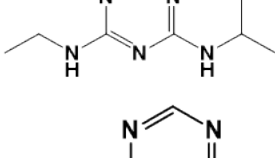
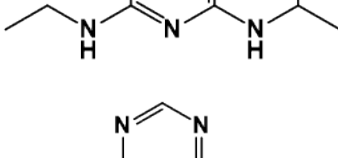
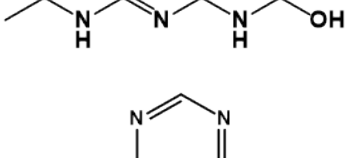
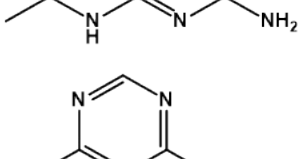
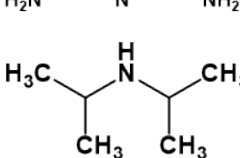

Anode	R_s (Ω)	R_{CT} (Ω)	R_{MT} (Ω)
ATO@Ti	2.53	5.78	1.56 ^a
BDD	3.84	30.12	17.34 ^a
EF-ATO	4.01	6.78	11.79

R_s : solution resistance. R_{CT} : charge transfer resistance. R_{MT} : mass transfer resistance.

^a For catalyst-coated planar ATO-Ti and BDD, R_{MT} is replaced by R_{int} (interfacial resistance).

Table S5. Intermediate products of the degradation of ATZ detected by UPLC-MS-MS.

Name	Chemical formula	Structural formula	m/z
ATZ	$C_8H_{14}ClN_5$		216
P1	$C_8H_{14}ClN_5O$		232
P2	$C_8H_{12}ClN_5O$		230
P3	$C_8H_{15}N_5O$		199
P4	$C_8H_{13}N_5O_2$		212
P5	$C_6H_{11}N_5O$		170
P6	$C_5H_8ClN_5O$		190
P7	$C_3H_5N_5O$		128
P8	$C_5H_8ClN_5$		174

P9	$C_6H_{10}ClN_5$		188
P10	$C_3H_4ClN_5$		146
P11	$C_3H_4N_4O_2$		129.2
P12	$C_3H_3N_3O_3$		130
P13	$C_3H_3N_3O_2$		114
P14	$C_9H_{17}N_5$		195.1
P15	$C_8H_{15}N_5$		182.9
P16	$C_6H_{11}N_5O$		172
P17	$C_5H_{11}N_5$		142
P18	$C_3H_7N_5$		114
P19	$C_6H_{15}N$		100

Supplemental References

- 1 C. Yang, S. Shang, L. Lin, P. Wang, Z. Ye, Y. Wang, K. Shih, L. Sun and X.-y. Li, *Nat. Water*, 2024, **2**, 793-802.
- 2 K. N. Van, H. T. Huu, V. N. Nguyen Thi, T. L. Le Thi, D. H. Truong, T. T. Truong, N. N. Dao, V. Vo, D. L. Tran and Y. Vasseghian, *Chemosphere*, 2022, **289**, 133120.
- 3 K. Liu, B. Jin, W. Han, X. Chen, P. Gong, L. Huang, Y. Zhao, L. Li, S. Yang, X. Hu, J. Duan, L. Liu, F. Wang, F. Zhuge and T. Zhai, *Nat. Electron.*, 2021, **4**, 906-913.
- 4 R. Zhang, Q. Wang, J. Zhang, Q. Lu, W. Liu, S. Yin and W. Cao, *Nanotechnology*, 2019, **30**, 434001.
- 5 J. Chen, Z. Chen, X. Zhang, X. Li, L. Yu and D. Li, *Appl. Catal. B: Environ.*, 2017, **210**, 379-385.
- 6 Y. Ji, C. Dong, D. Kong and J. Lu, *J. Hazard. Mater.*, 2015, **285**, 491-500.
- 7 Y. Deng, Z. Zhou, H. Zeng, R. Tang, L. Li, J. Wang, C. Feng, D. Gong, L. Tang and Y. Huang, *Appl. Catal. B: Environ.*, 2023, **320**, 121942.
- 8 B. Xue, B. Wang, J. y. Wang and J. Sun, presented in part at the 2010 4th International Conference on Bioinformatics and Biomedical Engineering, Chengdu, China, 18-20 June 2010, 2010.
- 9 S. Chen, P. He, X. Wang, F. Xiao, P. Zhou, Q. He, L. Jia, F. Dong, H. Zhang, B. Jia, H. Liu and B. Tang, *Chemosphere*, 2021, **268**, 128799.
- 10 N. Oturan, E. Brillas and M. A. Oturan, *Environ. Chem. Lett.*, 2012, **10**, 165-170.
- 11 Y. He, L. Wang, Z. Chen, X. Huang, X. Wang, X. Zhang and X. Wen, *J. Membrane Sci.*, 2022, **648**, 120362.
- 12 I. M. D. Gonzaga, A. R. Dória, R. S. S. Castro, M. R. R. Souza, M. A. Rodrigo, K. I. B. Eguiluz and G. R. Salazar-Banda, *Electrochim. Acta.*, 2022, **426**, 140782.
- 13 F. Zaviska, P. Drogui, J.-F. Blais, G. Mercier and P. Lafrance, *J. Hazard. Mater.*, 2011, **185**, 1499-1507.
- 14 P. Gayen, C. Chen, J. T. Abiade and B. P. Chaplin, *Environ. Sci. Technol.*, 2018, **52**, 12675-12684.
- 15 X. Xie, J. Zhao, S. Liang, X. He, C. Yu, R. Xie, J. Xu, L. Yang, D. Cheng and H. Lin, *Electrochim. Acta.*, 2023, **463**, 142819.
- 16 K. Yang, H. Lin, J. Jiang, J. Ma and Z. Yang, *Sep. Purif. Technol.*, 2022, **297**, 121453.